A Multi-optical Collector of Sunlight Employing Luminescent Materials and Photonic Nanostructures

Submitted to ADVANCED OPTICAL MATERIALS

DOI: 10.1002/adom.((please add manuscript number))
Article type: Full Paper

A Multi-Optical Collector of Sunlight Employing Luminescent Materials and Photonic Nanostructures

Author(s), and Corresponding Author(s)

Angelo Bozzola, Valentina Robbiano, Katia Sparnacci, Giulia Aprile, Luca Boarino, Antonio Proto, Roberto Fusco, Michele Laus, Lucio Claudio Andreani, Davide Comoretto

Angelo Bozzola[(a)], Lucio Claudio Andreani[(b)]
Dipartimento di Fisica, Università degli Studi di Pavia, via Bassi 6, I-27100, Pavia, Italy
e-mail: [(a)] angelobozzola@gmail.com
[(b)] lucio.andreani@unipv.it

Valentina Robbiano, Davide Comoretto[(c)]
Dipartimento di Chimica e Chimica Industriale, Università degli Studi di Genova,
via Dodecaneso 31, I-16146, Genova, Italy
e-mail: [(c)] davide.comoretto@unige.it

Katia Sparnacci, Michele Laus
Dipartimento di Scienze ed Innovazione Tecnologica, Università del Piemonte Orientale, via T. Michel 11, I-15100 Alessandria

Giulia Aprile, Luca Boarino
Quantum Research Labs & Nanofacility Piemonte, Electromagnetism Division,
Istituto Nazionale di Ricerca Metrologica, Strada delle Cacce 91, I-10135 Turin, Italy

Antonio Proto, Roberto Fusco[(d)]
Eni S. P. A., Centro ricerche sulle energie non convenzionali,
via Fauser 4, I-28100, Novara, Italy
e-mail: [(d)] roberto.fusco1@eni.com

Keywords: solar energy, light harvesting, luminescent concentrators, fluorescent concentrators, luminescence, diffraction, photonic structures

Abstract

We propose a multi-functional, semitransparent photovoltaic device for harvesting sunlight over a tunable spectral range extending from the UV to the IR. Self-assembled monolayers of nanospheres applied to luminescent concentrators provide a photon management architecture which relies on luminescence and diffraction of light. The light

diffraction is carefully tuned by changing the sphere diameter to match the transparency region of the fluorophores. The importance of each optical mechanism is inferred from a systematic experimental investigation of the External Quantum Efficiency of fabricated devices, and from the calculation of the resulting photocurrent under the AM 1.5 solar spectrum. Compared to the conventional luminescent concentrator, we show relative photocurrent improvements between 50 and 500% depending on the spectral properties of the device components. We demonstrate how to tailor the photovoltaic performances, the color and the degree of transparency of the device to provide a versatile photovoltaic unit for sustainable building-integrated applications.

1. Introduction

In this work we present a novel concept for collection and harvesting of solar radiation, which relies on two optical effects: luminescence and diffraction. The target is to demonstrate that these mechanisms can be properly combined into a semitransparent device, which stands as a good candidate for building-integrated applications. Building-integrated Photovoltaics (BIPV) represents an evolution in terms of solar energy harvesting and building construction. Some external parts of buildings, such as facades, glass walls, windows and skylights, are redesigned as solar power modules rather than just conventional elements for internal day lighting.[1-5] Urban environments pose an open challenge for the integration of Photovoltaics, as their energy consumption is very high and the integration of conventional solar panels may be critical. This work constitutes a step in this direction.

From the point of view of the research in materials science, optics, and energy systems, BIPV opens new possibilities in the field of advanced materials and smart optical design. In conventional solar cells based on opaque semiconductors such as silicon, sunlight has to be fully absorbed, and converted into electricity with the highest possible conversion efficiency.

For a semitransparent, building-integrated device, instead, the paradigm is different. Only a fraction of the incident sunlight has to be converted into electricity, while the rest is transmitted through the device and used for lighting. From the point of view of optics, a major challenge is to find a device architecture that allows for partial transparency and broadband light harvesting at the same time.

In the field of solar energy, luminescent materials are commonly employed in the so-called luminescent solar concentrators (LSCs).[6-15] A conventional LSC consists of a few millimeters thick plastic waveguide which is doped with one or more luminescent compounds. These compounds absorb sunlight in a given spectral range, and emit light at a lower energy: The device is therefore semitransparent. The emitted light that undergoes total internal reflection (TIR) propagates in the waveguide and, if it is not scattered outside the waveguide or re-absorbed by the luminescent compound, it reaches the edges. If solar cells are placed at these edges, light is converted into electricity. Despite the energy conversion efficiency of LSCs[16] being lower than for conventional solar cells made of inorganic semiconductors, they have several points of advantage for integration in the urban environments. In fact, the possibility of using cheap and low weight materials for the waveguides and chromophores,[11] the partial transparency of these devices, and the possibility of tuning their colors[17] are all key factors for the integration in novel-architecture buildings.

A major drawback of conventional LSCs is the limited spectral range for the absorption of sunlight, which results in a low conversion efficiency. To enable an efficient collection of sunlight, the luminescent compounds need a quantum yield (QY) approaching unity and a small spectral overlap between the absorption and emission bands in order to reduce self-absorption.[18] Up to now, only materials absorbing in the UV and in part of the visible spectral range meet these requirements.[11,19-21] Although a relatively high conversion efficiency exceeding 7% has been reported for bi-layer LSCs including two luminescent

materials absorbing in the visible,[16,22] the lack of efficient IR emitters limits the applicability of luminescence to the higher energy portion of the solar spectrum.

To harvest the photons with lower energy, we modify the conventional LSC architecture by including a monolayer of self-assembled nanospheres. This photonic structure is designed to promote forward diffraction into the transparent slab waveguide forming the LSC at wavelengths that are not absorbed by the luminescent compound.[23]

Nanostructured dielectric materials already proved to be a highly effective solution for improving light harvesting in solar cells based on weak absorbers.[24-29] Photonic structures have also been proposed for application into LSCs. For example, 1D photonic structures such as distributed Bragg reflectors or rugate filters,[30,31] dichroic and liquid crystal cholesteric mirrors,[32,33] as well as 3D structures such as opals layers[30,34] have been proposed to prevent the loss of light from the escape cones determined by the condition for TIR. 3D opals layers can be grown or applied to the LSCs, and the luminescent materials can be directly incorporated in the photonic lattice.[35,36] In this way, the opals modify the angular emission profile of the chromophore (which is typically isotropic), enhancing the coupling of emitted light into the waveguide. *It is worth remarking that all these approaches reported in the literature are not intended as ways to broaden the spectral response, but rather to increase the optical path of light in the sample and / or to reduce the waveguide optical losses.* Using these strategies, the spectral response can be higher than in the conventional LSCs without nanostructures, but the spectral range is still limited to the absorption band of the luminescent compound.[32] On the contrary, the main point of novelty of this work consists in the merging of luminescence and optical diffraction to improve the spectral response of the device in the range of wavelengths that are not absorbed by the luminescent materials. The final result is a new semitransparent photovoltaic device, which might be a good candidate for sustainable building-integrated applications.

2. Results and discussion

A sketch of the proposed hybrid LSC is shown in **Figure 1**. A polymethylmethacrylate (PMMA) slab is doped with an organic luminescent compound dispersed in the bulk. The slab constitutes the LSC, which is the first key element of the device. This is reported as an orange slab in Figure 1.

The second key element is a monolayer of polystyrene (PS) nanospheres, with diameters ranging from 298 to 801 nm, cast on a thin glass substrate. The four lateral edges of the LSC are covered with silicon photovoltaic (PV) cells. Ordered monolayers floating on the water surface (**Figure 2**a) are transferred to glass substrates (Fig. 2b). The corresponding SEM image (Fig. 2c) shows a rather compact arrangement in two dimensions. Disordered structures are instead obtained by spin-coating (Fig. 2d-2g). The degree of order in the sample determines the dominance of diffraction of light over scattering or vice versa. Ordered samples with uniform covering are characterized by clear diffraction effects both in reflection and in transmission, providing strong iridescence as observed in Figures 2a, 2b and 2d. Samples obtained with high frequency spin-coating, instead, are disordered and only partially covered. The result is a weak interaction of light with the photonic structure, and the lack of a diffraction pattern (Fig. 2f).

To evaluate the photovoltaic performance of the proposed device, we parallel connect the four lateral PV cells, and we measure the external quantum efficiency (EQE). Three configurations are investigated: a bare LSC doped with benzothiadiazole (DTB - see the Experimental Section and Supplementary Information), a transparent PMMA slab with a monolayer of spheres, and the proposed hybrid device with LSC and monolayer. The measured EQE spectra are reported in **Figure 3**. The total photocurrent per unit area of the LSC slab is calculated as:

$$J_{sc} = e\int_{350nm}^{1100nm} EQE(\lambda)\phi_{AM1.5}(\lambda)d\lambda, \quad (1)$$

where *e* denotes the elementary charge, and $\phi_{AM1.5}(\lambda)$ is the AM 1.5G photon flux,[37] which is reported in Figure 3 with a thin grey line. The range of integration is limited by the band gap of the silicon PV cells at the edges, and by the experimental setup.[38] A sketch of the different investigated configurations and the estimated J_{sc} are also reported in Figure 3. The EQE of the bare LSC (orange dashed curve in Figure 3) is around 0.5 in the band of absorption of the luminescent dye, between 350 and 550 nm. However, this absorption range is rather small compared to the useful solar spectrum, and relatively poor of photons compared to the NIR region. This limits the photogenerated current J_{sc} to only 3.36 mA/cm^2.

On the other hand, the transparent slab covered with the monolayer of spheres (diameter d=574 nm) is characterized by a much broader spectral response, which is limited in the low-energy region only by the lateral PV cells. The EQE spectrum spans the entire useful range of solar radiation, and it is also reported in Figure 3. The EQE never reaches the top value of the case of the bare LSC, and this is the key ingredient for the partial transparency. We note that the EQE is high from about 574 nm and 850 nm, with two maxima at $\lambda \sim 625$ nm and $\lambda \sim 775$ nm. These features can be explained as arising from forward diffraction of light in the transparent PMMA slab. The maximum wavelength (cut-off) for the first diffraction order can be estimated considering the wavevector of incident sunlight, the fundamental reciprocal lattice wavevector, and the real part of the refractive index of the PMMA slab (n_{PMMA}=1.45). At normal incidence in air along the z-direction of Figure 1, the amplitude of the incident wavevector in air writes as $K_{inc} = 2\pi/\lambda$. When first-order diffraction is considered, the amplitude of the planar component of the wavevector is equal to the first reciprocal vector, $K_{//} = 2\pi/d$. For propagating diffracted waves to exist in the PMMA slab, the square amplitude of the z-component of the wavevector must be real and positive, therefore $K_z^2 = (n_{PMMA} \cdot K_{inc})^2 - (2\pi/d)^2 > 0$. In terms of incident wavelength, the cut-off for diffraction in PMMA thus writes as:

$$\lambda < n_{PMMA} \cdot d. \quad (2)$$

The cut-off for backward diffraction in air, instead, is at higher energy and may be written as:

$$\lambda < d. \quad (3)$$

These cut-off values are indicated in Figure 3 with vertical dashed lines for the case of a monolayer of spheres with diameter d=574 nm arranged in an ideal defect-free triangular lattice. By substituting the proper values in Equations (2) and (3), we see that the range of high EQE corresponds to the range where only diffraction in PMMA takes place. For wavelengths shorter than the lattice period, back-diffraction is active and acts as an additional optical loss, thus limiting the EQE. For this device configuration, the resulting calculated photocurrent J_{sc} is 5.35 mA/cm^2, which is even higher than the previous case of the bare LSC.

The proposed hybrid device consists of the same LSC combined with the same monolayer of the previous example. The corresponding EQE is also reported in Figure 3. The resulting calculated J_{sc} is 7.21 mA/cm^2, which corresponds to a relative 115% enhancement compared to the case of the bare LSC. We note that the EQE and J_{sc} of the hybrid device are not exactly the sum of the correspondent quantities of the bare LSC and of the transparent slab covered with nanospheres. In fact, in the range of absorption of the luminescent compound, the EQE is slightly smaller than for the case of the bare LSC. The photonic structure induces scattering of the emitted light that propagates through the waveguide, and increases the optical losses. The final efficiency is the result of opposite mechanisms: improved in-coupling of light at low energy, and weak waveguide losses at high energy as well as backward diffraction. The gain obtained with diffraction at low energy is much larger than the high-energy losses. This proves that the simultaneous application of luminescence and diffraction of light improves the energy harvesting compared to the conventional LSC architecture.

Diffraction of light is a wavelength-selective process which relies on the long range order in the nanospheres layer. A perfectly ordered monolayer is just an idealized theoretical case-study. Every real structure is characterized by some degree of disorder, and this might affect the optical properties and the photovoltaic performance of the device. Among the various techniques for the fabrication of monolayers of nanospheres, the spin-coating allows to control the amount of disorder in the photonic lattice by simply changing the spinning frequency, nanosphere concentration and suspension viscosity. The effects of disorder can thus be investigated in a systematic and reproducible way. In this view, we prepare monolayers of spheres with diameter d=574 nm cast by the spin-coating technique at different rotation frequencies (three batches of different spheres concentration). These photonic structures are applied to the same LSC as previously described. For each sample, we measure the EQE and calculate the corresponding J_{sc}. Results are reported in **Figure 4**. From the EQE measurements summarized in Figure 4a, we observe two main effects: (i) samples obtained at small frequency (up to 30 rps) show qualitatively the same diffraction pattern observed in Figure 3 for the monolayers prepared by floating, and (ii) this pattern disappears for frequencies above 30 rps, and the entire EQE diminishes by increasing the spinning frequency. The vanishing of the diffraction pattern is due to the progressive destruction of the in-plane order. Also the surface covering is affected by the spinning frequency, as it is evident from the SEM top image reported in Figure 2g. This refers to a sample obtained by spin coating with the same sphere concentration used for the case of Figure 2e, but with a frequency of 50 rps instead of 20 rps. For the high-frequency samples most of the incident light does not interact with the photonic structure, and this determines a low EQE. The weaker interaction of light with the spheres is confirmed also by the EQE trend in the range of absorption of the luminescent material, which is reported in the inset of Figure 4a. In this spectral region, the EQE for high frequency samples is higher than for the low frequency ones. This is due to the

partial covering of the waveguide, which leads to a weaker interaction of the guided light with the photonic structure and reduced propagation losses. The results in terms of the J_{sc} are summarized in Figure 4b, where a monotonic decay is observed upon increasing the spinning frequency. The best achieved configuration from the point of view of light harvesting is the one obtained at 10 rps, which is the minimum allowed by our spin-coating setup. The sample has to be totally covered. Diffraction has to play an important role, leading to clear peaks in the EQE spectra. A moderate amount of disorder broadens the diffraction peaks, and allows the harvesting of photons with energy below the diffraction cut-off in the PMMA. This is beneficial for the global performance of the PV device. When disorder becomes dominant (and the surface covering incomplete), the estimated J_{sc} drops down to the value of the bare LSC.

We investigate now the role of the spheres diameter on forward diffraction inside the LSC slab. Several monolayers of PS nanospheres with diameters in the range 298-801 nm are deposited on glass with the floating method. To evaluate the relative importance of luminescence and diffraction, we consider three types of LSCs, each doped with a different luminescent compound: DPA, DTB,[39] and Lumogen F305 Red® by BASF. These materials absorb in the UV and visible ranges and emit light at lower energy. For simplicity, according to the emission spectrum the chromophore, LSCs are classified as blue, yellow, and red. The yellow LSC has already been used in the previous proof-of-concept. The chemical structures and the absorption / fluorescence properties of the employed dyes are given in Experimental Section and in the Supplementary Information (Fig. SI1).

The spheres diameter is the main parameter affecting the optical properties of the photonic structure, in particular the scaling cut-off wavelengths for forward and backward diffraction. To elucidate this point, we consider monolayers of spheres with different diameters coupled to the yellow LSC. The measured EQE spectra are reported in **Figure 5**.

The trends of the EQE for increasing diameter are marked with black arrows. Consistently with Equations (2) and (3), we note that the spectral range for diffraction in the PMMA red-shifts upon increasing the spheres diameter. This is in line with previous findings by some of us concerning the scaling of the optical properties of monolayers with the sphere size.[40,41] Spheres with a small diameter (especially 298 nm and 329 nm) are not the optimal solution in terms of light harvesting, as forward diffraction is limited to a spectral range where light is already absorbed by the luminescent compound. To take advantage of the additional optical mechanism of the hybrid collector, the spectral range for forward diffraction must not totally overlap with the absorption band of the luminescent dye. This is obtained by increasing the spheres diameter. Also in this case we observe that larger spheres lead to increased waveguide losses and back diffraction in the range of absorption of the chromophore (inset of Figure 5). However, the gain due to non-resonant diffraction largely overcomes these resonant losses, therefore the hybrid device is more performing than the bare LSC.

To evaluate the contributions of luminescence and of diffraction, we also consider various types of waveguides, either transparent or doped with different luminescent compounds (see **Figure SI1** for spectral details). To evaluate the sole contribution of luminescence to the photovoltaic performance, we first consider the bare blue, yellow and red LSCs with no photonic structures. Pictures of these LSCs are reported in **Figures 6**a, 6b, and 6c, respectively. The corresponding J_{sc} calculated from the EQE data are reported in Figure 6e with horizontal dashed lines. The photogenerated current is only 0.84 mA/cm^2 for the blue LSC, and it increases up to 3.36 mA/cm^2 and to 5.78 mA/cm^2 for the yellow and red LSCs, respectively. The photocurrent increases upon moving to dyes that absorb a larger portion of the visible sunlight.

To evaluate the maximum contribution of diffraction, we couple monolayers with different sphere diameters to a transparent PMMA slab. This slab is shown in Figure 6d and it

is used also in Figure 3. We measure the EQE, and calculate the corresponding J_{sc}. Results are reported in Figure 6e. Spheres with diameter d=574 nm give the maximum J_{sc} of 5.36 mA/cm^2.

Finally, we measure the EQE of hybrid devices obtained coupling the blue, yellow, and red LSCs to the same monolayers considered in the previous case. Results are reported in Figure 6e. For the hybrid device obtained with the blue LSC, diffraction plays a major role. The maximum J_{sc} is 5.35 mA/cm^2, and the optimal diameter is 702 nm. The relative improvement obtained with nanospheres compared to the bare blue LSC is approximately 530%. This giant enhancement is due to the small contribution of luminescence. In fact, this chromophore absorbs only in the UV range (Figure SI1), which is poor of solar photons. The situation is different for the other dyes. The hybrid device obtained with the yellow LSC reaches a maximum J_{sc} of 7.52 mA/cm^2 for the case of spheres with a diameter of 801 nm. The relative improvement compared to the bare yellow LSC is +124%. The hybrid collector obtained with the red LSC, instead, reaches a maximum J_{sc} of 8.95 mA/cm^2, with a relative +55% improvement. The optimal sphere diameter is again 801 nm. In this case, luminescence gives the major contribution to the global photovoltaic performance. The calculated photocurrent, relative enhancement and optimal sphere diameters are summarized in **Table 1** for all the investigated configurations.

Interestingly, we note that the optimal spheres diameter moves in the range 700-800 nm (at the upper bounds of our experimental range) when diffraction is coupled with luminescence. The shift can be explained in the light of the results of Figure 5. For the case of the transparent slab with the monolayer, the optimal period (574 nm) gives diffraction in the PMMA for the central wavelengths of the useful solar spectrum (which extends from approximately 350 to 1100 nm, since we are using silicon PV cells). For the cases of the hybrid devices, a part of this useful spectrum is absorbed by the dye, and only the low energy

portion needs to be coupled to the waveguide. To accomplish this, the spheres diameter has to be increased up to 700-800 nm, as it is shown in Figure 6e.

The results of this section demonstrate that our concept of multi-optical device can be implemented with different types of luminescent materials. The inclusion of diffraction always results in an improved photovoltaic performance compared to the case of the bare LSC. To meet the requirements imposed by the chromophores, the spectroscopic response of the photonic structures can be properly tuned. For the case of the monolayers of spheres, the tuning is done by simply changing the spheres diameter. In this way, the spectral ranges of active absorption and forward diffraction do not overlap, and the photocurrent is maximized. The use of lateral PV cells working deeper in the Near Infrared further allows to improve the device efficiency when even larger nanospheres are used.

Our results are promising from the point of view of building integration and architectural design. Indeed, while the visual impact of facades, windows and walls can be tuned by the absorption spectrum of the dye embedded inside the LSC, the photovoltaic efficiency can be improved by light diffraction of NIR photons, which are however not detected by our eyes. In this way, the transparency in the visible is not affected by the diffractive process, which nevertheless contribute to a higher conversion efficiency.

3. Conclusions

We proposed a novel, semitransparent photovoltaic device based on a luminescent solar collector covered with a monolayer of nanospheres. By taking advantage of luminescence and diffraction of light, we obtained a broadband light harvesting and a higher photocurrent compared to a bare LSC without photonic structure.

The photovoltaic performance of the hybrid collector has been experimentally investigated by means of EQE measurements. The device performance relies on two opposite effects: the increased spectral response at low energy due to diffraction, and minor waveguide losses that decrease the EQE in the absorption range of the luminescent compound. The first effect prevails and it yields a large enhancement of the photocurrent compared to the bare LSC. We demonstrated the versatility of our approach and we quantified the relative importance of each involved optical effect. By changing the diameter of the spheres, we tuned the optical response of the photonic structure according to the spectral properties of the dyes, and particularly the cut-offs wavelengths for diffraction in the PMMA and in air. The sphere diameter has to be large enough in order that the spectral range for forward diffraction (in the waveguide) does not totally overlap with the absorption band of the luminescent compound. This goal is achieved when using spheres with a diameter of the order of 700-800 nm. The maximum photocurrent enhancement due to the monolayer depends on the importance of luminescence in the global PV performance. For the case of the blue LSC, which absorbs only UV light, the enhancement exceeds 530%. Instead, for the yellow and red LSCs which absorbs also visible sunlight, we measured maximum improvements of 124% and 55%, respectively. Thanks to the improved efficiency combined with the partial transparency, the proposed device appears as a promising candidate for future high-efficiency building-integrated Photovoltaics.

4. Experimental section

Nanospheres synthesis

Nanosphere samples with mean diameters ranging from 298 to 574 nm were synthesized by surfactant-free emulsion polymerization of styrene. Different nanosphere

diameters were obtained by varying the amount of monomer, reported in Table 2, employed in the polymerization reaction. In detail, 700 mL of water were introduced in a 1 L five-neck jacketed reactor, equipped with a condenser, a mechanical stirrer, a thermometer and inlets for nitrogen and styrene. The reactor was purged with nitrogen for 20 min then the appropriate amount of styrene was added and the mixture was heated to 80°C. After 30 min of equilibration time, a potassium persulfate aqueous solution (10 mL, 0.92 mmol) was added and the mixture was reacted for 24 h. The obtained latex was purified from the unreacted monomer by dialyses.

Nanosphere samples with mean diameter of 702 and 801 nm were obtained by seeded emulsion polymerization starting from the sample with d=574 nm as the seed particle, and varying the amount of styrene (Table 2). In detail, 200 mL of latex containing 13.0 g of nanospheres with d=574 nm and 300 ml of water were introduced in a 1 L five-neck jacketed reactor. The reactor was purged with nitrogen for 20 min then the appropriate amount of styrene was added and the mixture was heated to 80°C. After 30 min of equilibration time a potassium persulfate aqueous solution (5 mL, 0.74 mmol) was added and the mixture was reacted for 24 h. The obtained latex was purified from the unreacted monomer by dialyses.

Nanosphere size and size distribution were measured by scanning electron microscopy (SEM) and by dynamic light scattering (PCS). The microscope was a Inspect F SEM-FEG (Field Emission Gun) from FEI company, with a beam diameter of 3 nm. The SEM micrographs were elaborated by the Scion Image processing program. From 300 to 350 individual microsphere diameters were measured for each sample. Dynamic light scattering analysis was performed at 25°C, with a Malvern Zetasizer 3000 HS at a fixed scattering angle of 90°, using a 10mV He–Ne laser and PCS software for Windows (version 1.34, Malvern, UK). Each value is the average of five measurements. The instrument was checked with a

standard polystyrene latex with a diameter of 200 nm. Table 2 reports the amount of styrene employed for each sample and the nanosphere size obtained by SEM and PCS analysis.

Monolayers preparation

Ordered monolayers of spheres were prepared through the self-assembling method at the air-water interface.[40,41] Nanospheres water suspensions were properly diluted with ethanol in the range 1-20 mg/ml with water:ethanol ratio in the range 1:1-1:7. The new suspensions were then dropped on a glass slide inserted into a water reservoir. A temporary alcohol-water bilayer was formed and nanospheres segregate into the alcoholic layer where they concentrate and flocculate leading to the formation of a well ordered two dimensional structure. Small amount of surfactant is added at the edges of the floating nanosphere island thus providing an additional compacting stimulus. Such structures were then transferred onto a clean soda lime glass slide (22×22 mm^2) dipped into the reservoir. All glass slides used in the work have been carefully cleaned by piraña solution. Disorderd monolayers were prepared by spin-coating.[59] Nanospheres water suspensions (5-90 □l) were dynamically or statically cast on glass slides by using a SCV spinner from from Novocontrol. The rotational speed spans the range 10–200 rotations per second (rps).

The luminescent solar concentrators under investigation

The LSCs used in this work are made of PMMA slabs Altuglas VS-UVT 100 (dimensions: 22×22×6 mm^3). For the cases of the blue, yellow, and red LSCs, PMMA is doped (100 ppm) with diphenylantracene (DPA), benzothiadiazole (DTB),[39] and with the BASF dye Lumogen F 305 Red®, respectively (their chemical structures are reported in

Figure SI1). Optical absorption spectra were collected at room temperature in transmission mode on a double beam and double monochromator Perkin Elmer Lambda 950 UV-VIS-NIR spectrophotometer. Photoluminescence emission and excitation spectra were acquired with a Horiba Jobin Yvon Fluorolog 3 spectrofluorometer, equipped with a 450 W Xenon lamp coupled to a single monochromator for excitation, a double monochromator for emission and with both a photomultiplier and a CCD detector. The absorption and emission spectra are reported in Figure SI1 (Supporting Information).

LSCs are obtained coupling these doped PMMA slabs to four crystalline silicon PV cells IXYS KXOB 22-12×1.[44] The lateral dimensions are 22×6 mm^2, and perfectly fit the dimension of the lateral facet of the PMMA slab. The PV cells and the glass covered with PS spheres are optically coupled to the LSC slab by means of a transparent gel based on silicone oil, which provides a good optical impedance matching.

External Quantum Efficiency measurements

The External Quantum Efficiency (EQE) is measured with a setup based on a 50 W halogen lamp as the light source, and an Acton monochromator model SP2150-i with 1200 rows/mm.[38] The incident monochromatic beam is split by means of a glass beam splitter with known reflectance and transmittance, and sent to the investigated device and to a calibrated detector. To measure EQE, the current signal of the investigated device is compared with the signal from the photodetector. For the detection, we used a Newport silicon calibrated photodiode model 818-UV (calibration range 350-1100 nm). The measurements are done at normal incidence; the spot size is 16×16 mm^2, and the direct illumination of the lateral PV cells is always avoided.

Received: ((will be filled in by the editorial staff))
Revised: ((will be filled in by the editorial staff))
Published online: ((will be filled in by the editorial staff))

[1] D. Prasad, M. Snow, *Designing with solar power. A source book for building integrated photovoltaics (BIPV).* (The Images Publishing Group, USA, 2005).

[2] A. Henemann, *Renewable Energy Focus* **2008**, *9*, 14, 16-19.

[3] D. Chemisana, *Renew. Sust. Energ. Rev.* **2011**, *15*, 603-611.

[4] B. Norton, P. C. Eames, T. K. Mallick, M. J. Huang, S. J. McCormack, J. D. Mondold, Y. G. Yohanis, *Solar Energy* **2011**, *85* 1629-1664.

[5] B. P. Jelle, C. Breivik, H. D. Røkenes, *Sol. Energ. Mater. Sol. C.* **2012**, *100*, 69-96 (2012).

[6] W. H. Weber, J. Lambe, *Appl. Optics* **1976**, *15*, 2299-2300.

[7] J. A. Levitt, W. H. Weber, *Appl. Optics* **1977**, *16*, 2684-2689.

[8] R. Reisfeld, S. Neuman, *Nature* **1978**, *274*, 144-145.

[9] J. S. Batchelder, A. H. Zewai, T. Cole, *Appl. Optics* **1979**, *18*, 3090-3110.

[10] J. S. Batchelder, A. H. Zewai, T. Cole, *Appl. Optics* **1981**, *20*, 3733-3754.

[11] M. G. Debije, P. P. C. Verbunt, *Adv. Energy Mater.* **2012**, *2*, 12-35.

[12] M. G. Debije, C. Menelaou, L. M. Herz, A. P. H. J. Schenning, *Adv. Opt. Mater.* **2014**, *2*, 687-693.

[13] Y. Zhao, G. A. Meek, B. G. Levine, R. R. Lunt, *Adv. Opt. Mater.* **2014**, *2*, 606-611.

[14] S. F. Daorta, A. Proto, R. Fusco, L. C. Andreani, M. Liscidini, *Appl. Phys. Lett.* **2014**, *104*, 153901.

[15] J. C. Goldschmidt, L. Prönneke, A. Büchtemann, J. Gutmann, L. Steidl, M. Dyrba, M. C. Wiegand, B. Ahrens, A. Wedel, S. Schweizer, B. Bläsi, R. Zentel, U. Rau, *Fluorescent Concentrators for Photovoltaic Applications*, in *Photon Management in Solar Cells* (eds R. B.

Wehrspohn, U. Rau and A. Gombert), Wiley-VCH Verlag GmbH & Co. KGaA, Weinheim, Germany (2015).

[16] M. A. Green, K. Emery, Y. Hishikawa, W. Warta, E. D. Dunlop, *Prog. Photovolt: Res. Appl.* **2015**, *23*, 1-9.

[17] M. G. Debije, *Adv. Funct. Mater.* **2010**, *20*, 1498-1502.

[18] M. Debije, *Nature* **2015**, *519*, 298-299.

[19] Y. Zhao, R. R. Lunt, *Adv. Energy Mater.* **2013**, *3*, 1143-1148.

[20] C. S. Erickson, L. R. Bradshaw, S. McDowall, J. D. Gilbertson, D. R. Gamelin, D. L. Patrick, *ACS Nano* **2014**, *8*, 3461-3467.

[21] F. Meinardi, A. Colombo, K. A. Velizhanin, R. Simonutti, M. Lorenzon, L. Beverina, R. Viswanatha, V. I. Klimov, S. Brovelli, *Nature Photon.* **2014**, *8*, 392-399.

[22] L. H. Slooff, E. E. Bende, A. R. Burgers, T. Budel, M. Pravettoni, R. P. Kenny, E. D. Dunlop, A. Büchtemann, *Phys. Stat. Sol. (RRL)* **2008**, *2*, 257-259.

[23] R. Fusco, L. C. Andreani, A. Bozzola, D. Comoretto, V. Robbiano, M. Laus, K. Sparnacci, Italian patent application MI2015A000091, *Dispositivo fotovoltaico a concentrazione ibrida*. Filing date: 27.01.2015.

[24] J. Zhao, A. Wang, M. A. Green, *Prog. Photovolt: Res. Appl.* **1999**, *7*, 471-474.

[25] C. Battaglia, J. Escarré, K. Söderström, M. Charrière, M. Despeisse, F. J. Haug, C. Ballif, *Nature Photon.* **2011**, *5*, 535-538.

[26] A. Polman, H. A. Atwater, *Nature Mater.* **2012**, *11*, 174-177.

[27] M. M. Moslehi, P. Kapur,J. Kramer, V. Rana, S. Seutter,A. Deshpande, T. Stalcup, S. Kommera, J. Ashjaee,A. Calcaterra, D. Grupp, D. Dutton, R. Brown, World-record 20.6% efficiency 156 mm × 156 mm full-square solar cells using low-cost kerfless ultrathin epitaxial silicon and porous silicon lift-off technology for industry-leading high-performance smart PV modules. PV Asia Pacific Conference (APVIA/PVAP), 24 October 2012.

[28] E. R. Martins, J. Li, Y. Liu, V. Depauw, Z. Chen, J. Zhou, T. F. Krauss, *Nature Commun.* **2013**, *4*, 2665.

[29] F. Priolo, T. Gregorkiewicz, M. Galli, T. F. Krauss, *Nature Nanotech.* **2014**, *9*, 19-32.

[30] J. C. Goldschmidt, M. Peters, L. Prönneke, L. Steidl, R. Zentel, B. Bläsi, A. Gombert, S. Glunz, G. Willeke, U. Rau, *Phys. Stat. Sol. a* **2008**, *205*, 2811-2821.

[31] J. Gutmann, M. Peters, B. Bläsi, M. Hermle, A. Gombert, H. Zappe, J. C. Goldschmidt, *Opt. Express* **2012**, *20*, A157-A167.

[32] W. G.J.H.M. van Sark, K. W. J. Barnham, L. H. Slooff, A. J. Chatten, A. Büchtemann, A. Meyer, S. J. McCormack, R. Koole, D. J. Farrell, R. Bose, E. E. Bende, A. R. Burgers, T. Budel, J. Quilitz, M. Kennedy, T. Meyer, C. De Mello Donegá, A. Meijerink, D. Vanmaekelbergh, *Opt. Express* **2008**, *16*, 21773-21792.

[33] M. G. Debije, M. P. Van, P. P. C. Verbunt, M. J. Kastelijn, R. H. L. van der Blom, D. J. Broer, C. W. M. Bastiaansen, *Appl. Opt.* **2010**, *49*, 745-751.

[34] J. C. Goldschmidt, M. Peters, J. Gutmann, L. Steidl, R. Zentel, B. Bläsi, M. Hermle, Increasing Fluorescent Concentrator Light Collection Efficiency by Restricting the Angular Emission Characteristic of the Incorporated Luminescent Material - the “Nano-Fluko” Concept. SPIE Photonics for Solar Energy Systems III SPIE Proc., 77250S-1 (2010).

[35] J. Gutmann, J. Posdziech, M. Peters, L. Steidl, R. Zentel, H. Zappe, J. C. Goldschmidt, SPIE Photonics for Solar Energy Systems IV, SPIE Photonics for Solar Energy Systems IV, SPIE Proc., pp 84381O-1 (2012).

[36] D.K.G.D. Boer, S.R.K. Rodriguez, S. L. Diedenhofen, *Luminescent solar concentrator with nanostructured luminescent layer.* International patent WO 2013/093696 A2. International publication date: 27.06.2013.

[37] The United States National Renewable Energy Laboratory (NREL) website. www.rrdc.nrel.gov/solar/spectra/am1.5/ (Accessed: April 2015).

[38] A. Bozzola, S. Flores Daorta, M. Galli, M. Patrini, L.C. Andreani, A. Alessi, R. Fusco, A. Proto, P. Scudo, Proceedings of the 26th EU PVSEC, paper 1.CV.3.10, 259-263. Hamburg, Germany, September 2011.

[39] A. Alessi, R. Fusco, A. A. Proto, G. Schimperna, P. Scudo, *Photoluminescent compositions for spectrum converters with enhanced efficiency*. International patent WO/2011/048458. Publication date: 28.04.2011. International filling date: 14.10.2010.

[40] V. Robbiano, M. Giordano, C. Martella, F. Di Stasio, D. Chiappe, F. Buatier de Mongeot, D. Comoretto, *Adv. Opt. Mater*. **2013**, *1*, 389-396.

[41] A. Belardini, A. Benedetti, M. Centini, G. Leahu, F. Mura, S. Sennato, C. Sibilia, V. Robbiano, M. C. Giordano, C. Martella, D. Comoretto, *Adv. Opt. Mater*. **2014**, *2*, 208-213.

[42] K. Sparnacci, D. Antonioli, S. Deregibus, M. Laus, T. Poggio, V. Kapeliouchko, *Macromolecules* **2009**, *42*, 3518-3524.

[43] D. Antonioli, S. Deregibus, G. Panzarasa, K. Sparnacci, M. Laus, L. Berti, L. Frezza, M. Gambini, L. Boarino, E. Enrico, D. Comoretto, *Polymer International* **2012**, *61*, 1294-1301.

[44] IXYS website: www.ixys.com/ProductPortfolio/GreenEnergy.aspx (Accessed: May 2015).

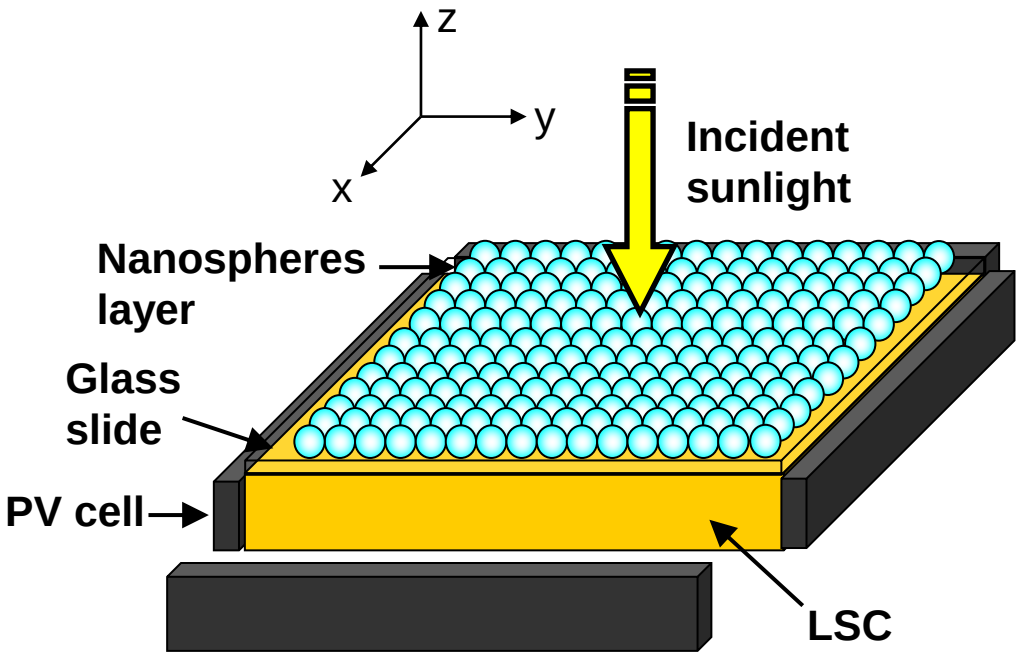

Figure 1. (Color online) Sketch of the proposed hybrid device: a LSC plate (orange slab) is doped with a luminescent material, and optically coupled to four lateral silicon PV cells (black rectangles) and to the transparent glass carrying the nanospheres layer (transparent slab with cyan spheres on the top).

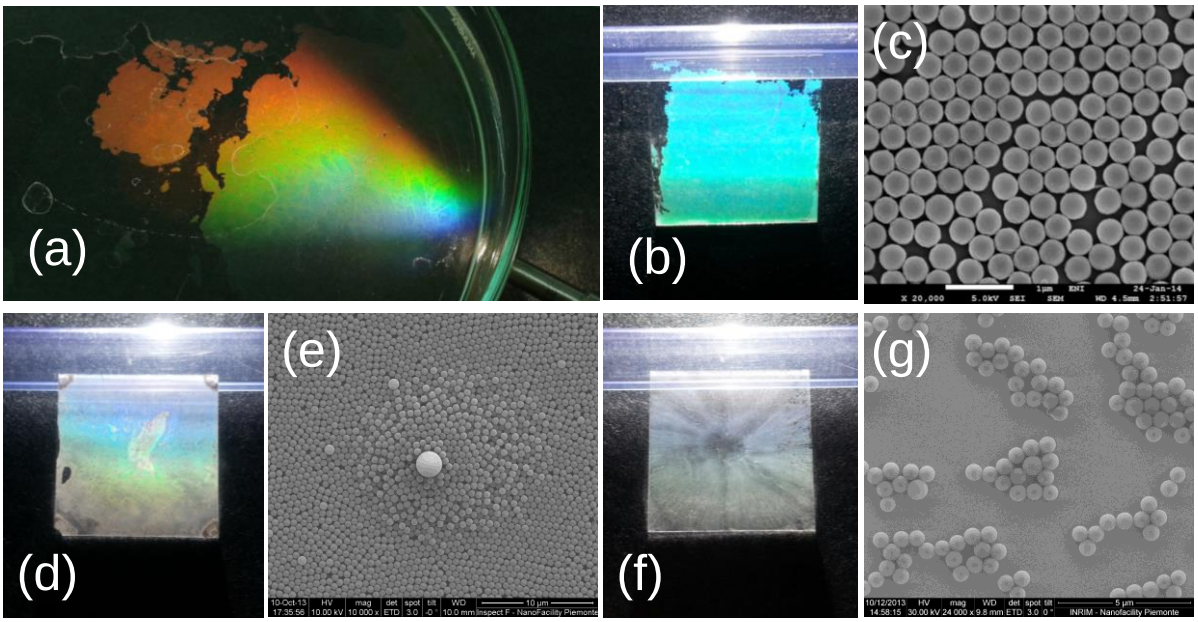

Figure 2. (Color online) The photonic structures under investigation. **(a)** Picture of a monolayer island made of PS spheres with diameter *d*=329 nm in water solution. **(b)** Picture of the resulting nanosphere film deposited on glass by self-assembling method, and **(c)** corresponding SEM image. **(d)** Picture of a film made of PS spheres with *d*=574 nm deposited on glass using spin-coating at 20 rps, and **(e)** corresponding SEM image. **(f)** Picture of a film made of PS spheres with *d*=574 nm deposited on glass using spin-coating at 50 rps, and **(g)** corresponding SEM image. In panels (b), (d), and (f) samples are illuminated at grazing incidence from the back.

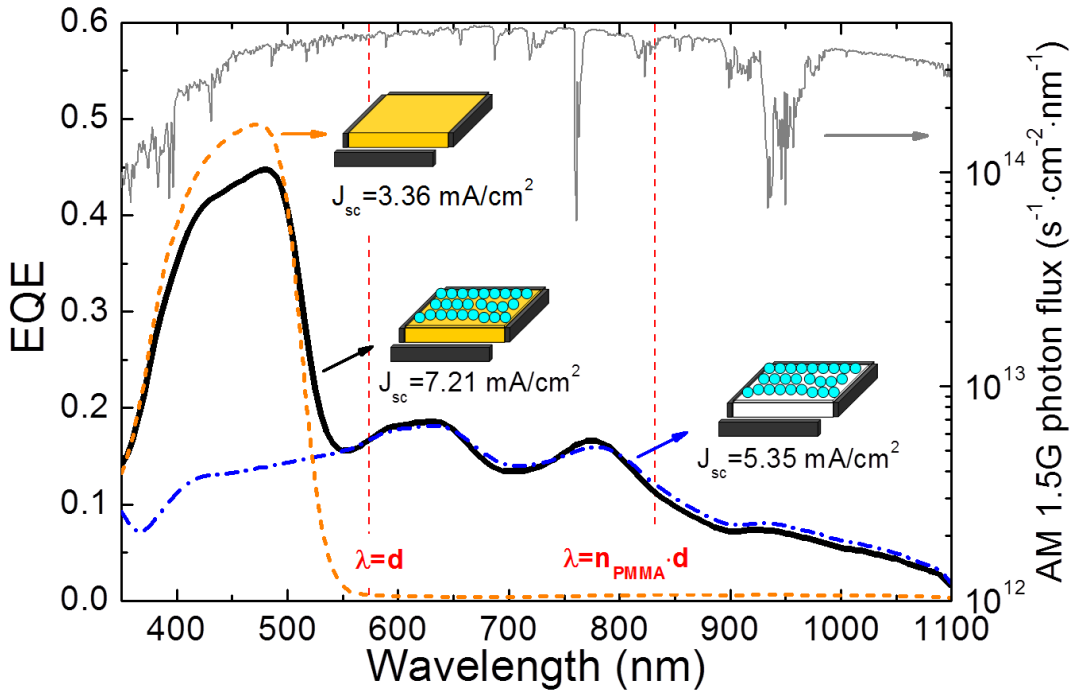

Figure 3. (Color online) Proof-of-concept of the proposed device. Measured External Quantum Efficiency (EQE) for a bare LSC doped with the organic luminescent dye DTB (orange dashed line), for a transparent PMMA slab with lateral PV cells and covered with a monolayer of PS spheres with *d*=574 nm (dashed and dotted blue line), and for the hybrid device where the same photonic structure is coupled to the aforementioned LSC (solid black line). The sketches of the devices under investigation and the calculated J_{sc} are also reported. The AM 1.5G solar photon flux is reported with a thin grey solid line.

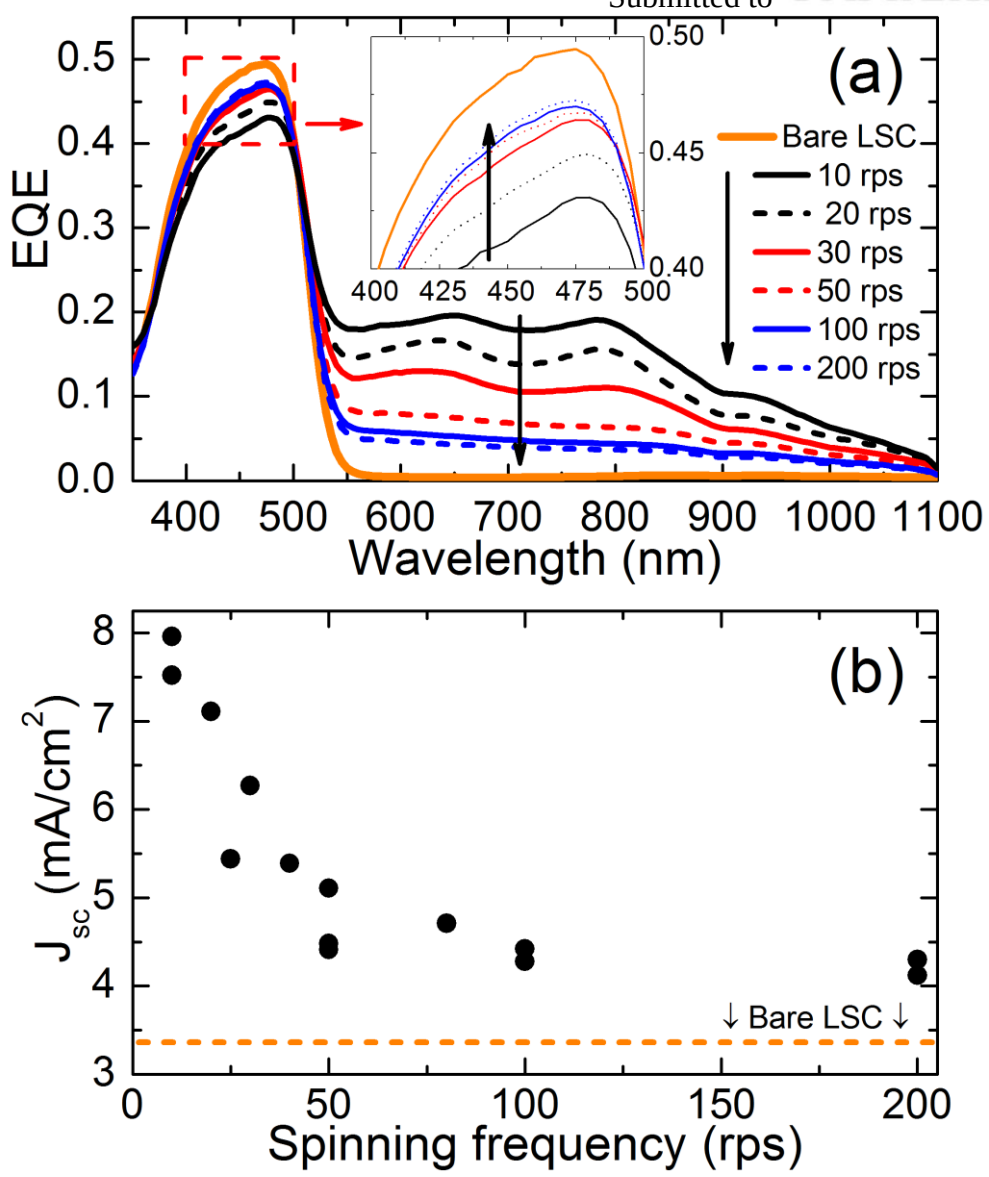

Figure 4. (Color online) Effects of the surface covering and disorder in the photonic structure on the photovoltaic performance. **(a)** Measured External Quantum Efficiency (EQE) for a bare LSC (orange solid line), and for the same LSC coupled to spheres layers deposited by spin-coating at different velocity (solid and dashed black, red, and blue lines). The trends for increasing spinning frequency are marked with black arrows. **(b)** J_{sc} calculated from the EQE data for the three investigated batches of samples coupled to the aforementioned LSC. The value of the J_{sc} for the bare LSC is reported with a horizontal dashed orange line.

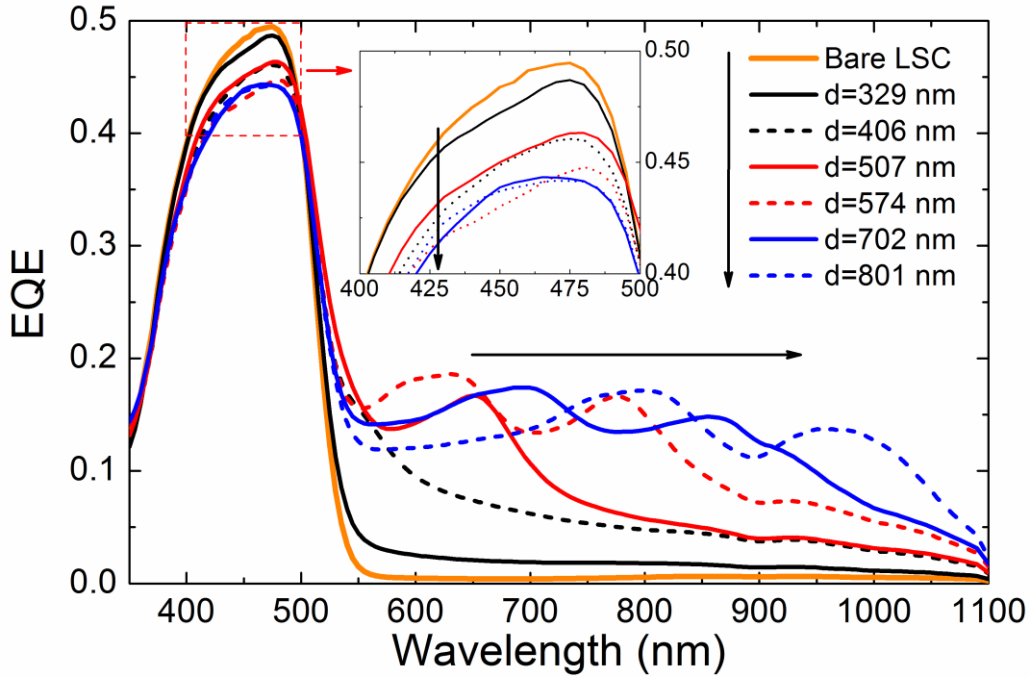

Figure 5. (Color online) Tuning of the optical diffraction. Measured External Quantum Efficiency (EQE) for a bare DTB-doped LSC (orange solid line), and for the hybrid device obtained coupling this LSC to PS spheres monolayers with different diameter *d* (solid and dashed black, red, and blue lines). The trends for increasing sphere diameter are marked with black arrows.

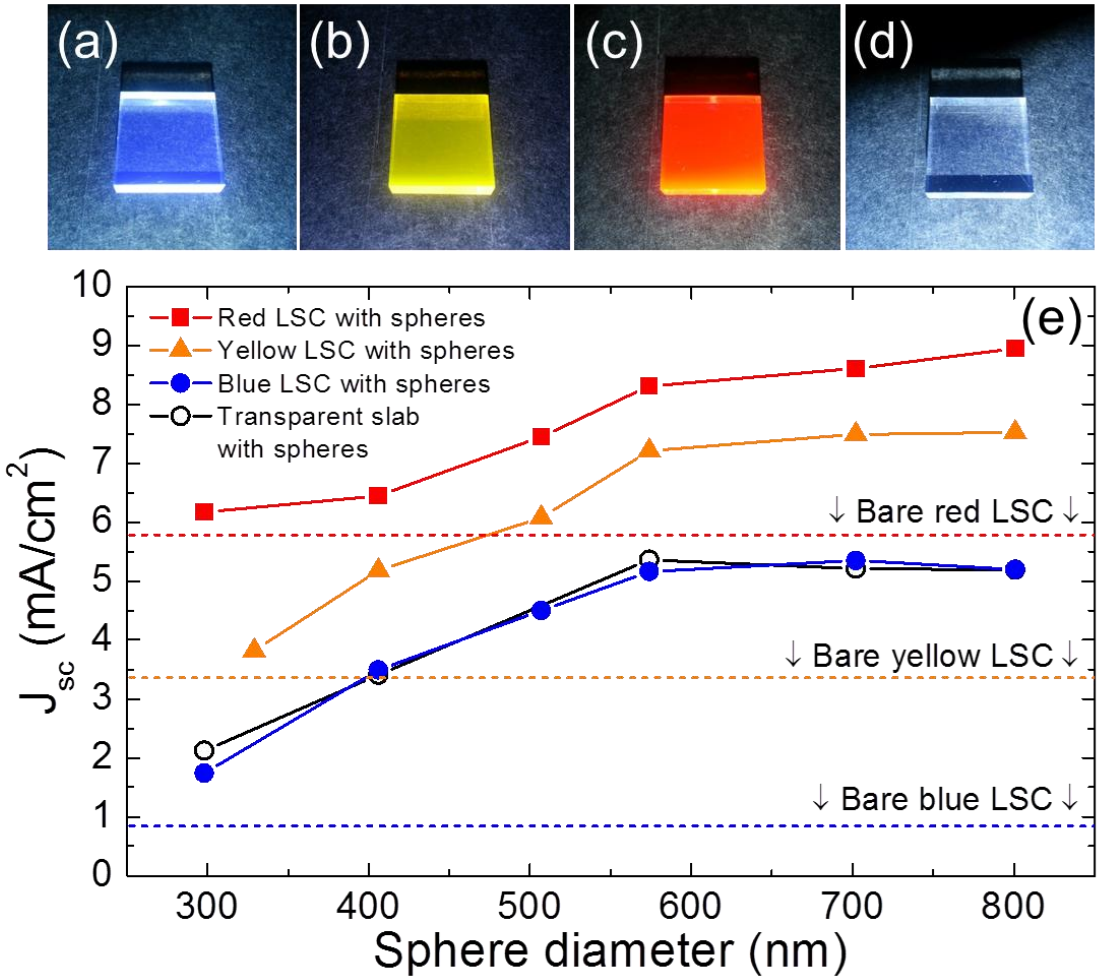

Figure 6. (Color online) Pictures of the investigated waveguides for LSCs and hybrid collectors: **(a)** a PMMA slab doped with DPA (blue), **(b)** DTB (yellow), **(c)** Lumogen F 305 Red® (red), and **(d)** a transparent PMMA slab. **(e)** J_{sc} values calculated from the measured EQE data for the bare blue, yellow, and red LSCs (dashed horizontal lines), for the transparent slab with nanospheres with different diameters (black line and opened symbols), and for the hybrid devices obtained coupling the blue, yellow, and red LSCs to the aforementioned nanospheres layers (colored lines and closed symbols).

Table 1. Main parameters for the bare LSCs and the hybrid devices obtained coupling different types of waveguides to monolayers of spheres obtained with the self-assembling method: short-circuit current densities for the bare LSC, for the optimized hybrid device, relative improvement compared to the bare LSC, and optimal sphere diameter.

Waveguide	**J_{sc} bare LSC (mA/cm^2)**	**J_{sc} hybrid device (mA/cm^2)**	**Relative enhancement compared to bare LSC**	**Optimal sphere diameter (nm)**
Transparent PMMA slab	-	5.36	-	574
PMMA slab + blue chromophore	0.84	5.35	+ 537%	702
PMMA slab + yellow chromophore	3.36	7.52	+ 124 %	801
PMMA slab + red chromophore	5.78	8.95	+ 55%	801

Table 2. Preparation details and characteristics of the nanosphere samples.

Sample	Styrene (ml)	Nanoparticle Diameter SEM (nm)	Nanoparticle Diameter PCS (nm)
1	30.0	298 ± 10	331 ± 6
2	50.0	329 ± 12	355 ± 5
3	80.0	406 ± 16	445 ± 7
4	100.0	507 ± 13	620 ± 6
5	120.0	574 ± 12	616 ± 8
6	15.0*	702 ± 13	847 ± 7
7	25.0*	801 ± 15	908± 5

***** Starting from 200 mL of latex containing 13.0 g of nanospheres with *d*=574 nm and 300 ml of water.

Table of contents entry.

We propose a multi-optical photovoltaic device based on a luminescent solar collector and on a photonic structure made of polystyrene nanospheres. Luminescence and diffraction of light are the key optical mechanisms for broadband light harvesting. By means of EQE measurements we investigate the effects of different chromophores and sphere diameters, optimizing the photovoltaic performance of the device.

Keywords: solar energy, light harvesting, luminescence, diffraction, photonic structures

Author(s), and Corresponding Author(s)

Angelo Bozzola[(a)], Valentina Robbiano, Katia Sparnacci, Giulia Aprile, Luca Boarino, Antonio Proto, Roberto Fusco[(b)], Michele Laus, Lucio Claudio Andreani[(c)], Davide Comoretto[(d)]

(a) e-mail: angelobozzola@gmail.com
(b) e-mail: roberto.fusco1@eni.com
(c) e-mail: lucio.andreani@unipv.it
(d) e-mail: davide.comoretto@unige.it

Title: A Multi-Optical Collector of Sunlight Employing Luminescent Materials and Photonic Nanostructures

ToC figure

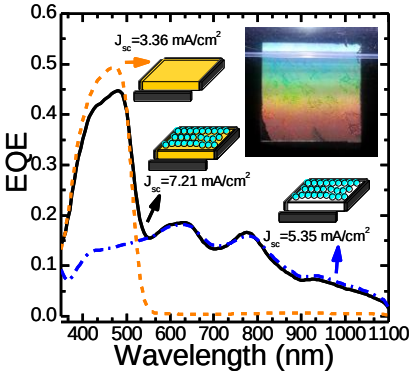

Submitted to ADVANCED OPTICAL MATERIALS

Supporting Information

for *Adv. Opt. Mater.*, DOI: 10.1002/adom.((please add manuscript number))

Title: A Multi-Optical Collector of Sunlight Employing Luminescent Materials and Photonic Nanostructures

Author(s), and Corresponding Author(s)
Angelo Bozzola[(a)], Valentina Robbiano, Katia Sparnacci, Giulia Aprile, Luca Boarino, Antonio Proto, Roberto Fusco[(b)], Michele Laus, Lucio Claudio Andreani[(c)], Davide Comoretto[(d)]

(a) e-mail: angelobozzola@gmail.com
(b) e-mail: roberto.fusco1@eni.com
(c) e-mail: lucio.andreani@unipv.it
(d) e-mail: davide.comoretto@unige.it

The absorption and emission spectra for the organic luminescent compounds used in this work are measured following the procedure of Section 4. These are reported in the panels (a) and (b) of **Figure SI1**. For DPA (Figure SI1a) and DTB (Figure SI1b) we report the measured molar extinction coefficients, which have units of cm-1 M-1. For the commercial dye Lumogen F 305 Red® (Figure SI1c), we report the absorption in arbitrary units. The External Quantum Efficiency (EQE) of silicon the solar cells applied to the lateral facets of the LSCs are measured following the procedure described in Section 4. The EQE spectrum is reported in Figure SI1, panel (d).

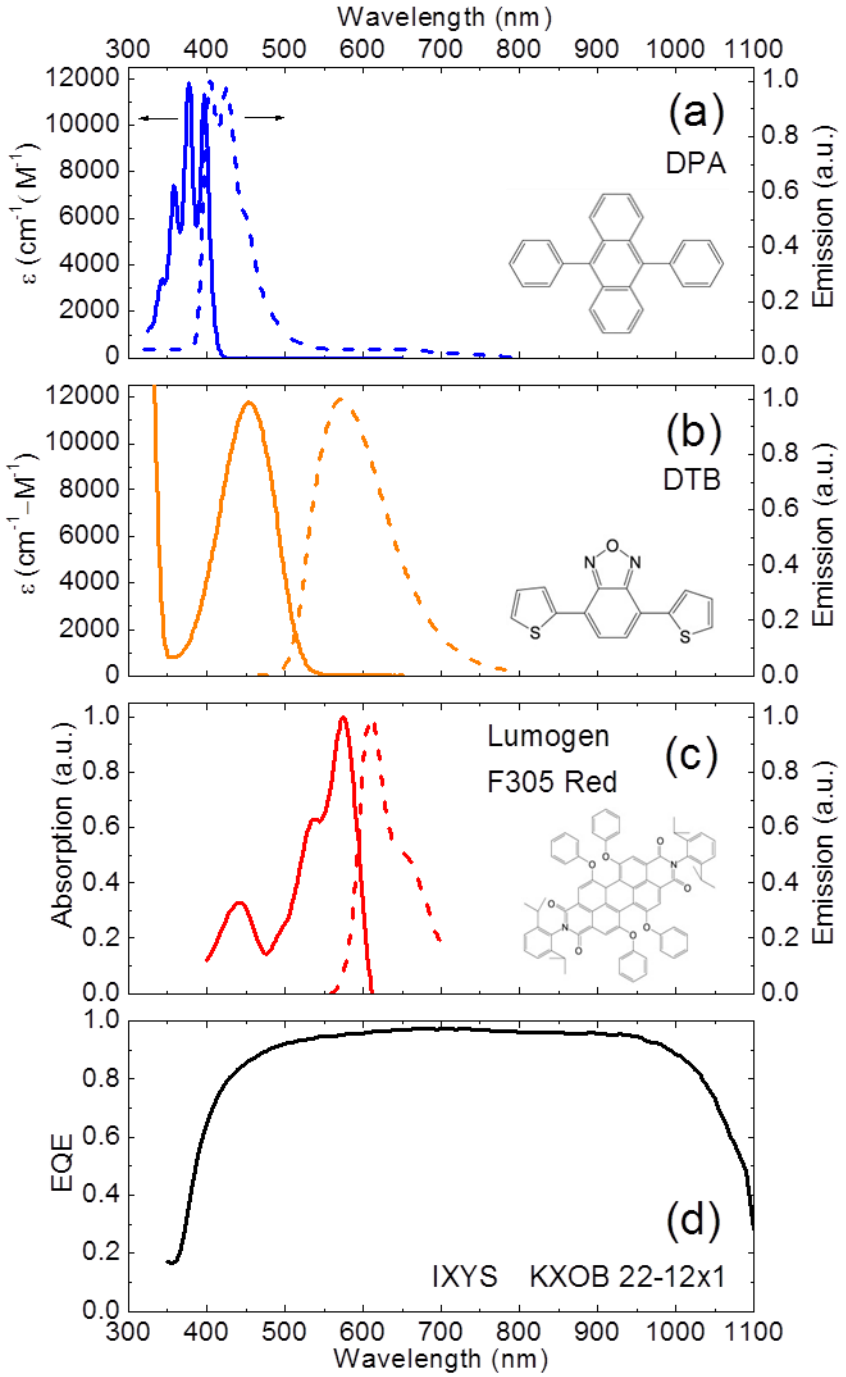

Figure SI1. (Color online) Absorption and emission spectra for the luminescent materials used in this work: DPA **(a)**, DTB **(b)**, and BASF Lumogen F 305 Red® **(c)**. Structural formulas of these compounds are also reported. **(d)** Measured External Quantum Efficiency for the silicon PV cells (IXYS KXOB 22-12x1) used in this work.